

Examining Experimental Raman Mode Behavior in Mono- and Bilayer 2H-TaSe₂ via Density Functional Theory: Implications for Quantum Information Science

Sugata Chowdhury, Heather M. Hill, Albert F. Rigosi, Andrew Briggs, Helmuth Berger, David B. Newell, Angela R. Hight Walker, and Francesca Tavazza*



Cite This: <https://dx.doi.org/10.1021/acsnano.0c03222>



Read Online

ACCESS |



Metrics & More



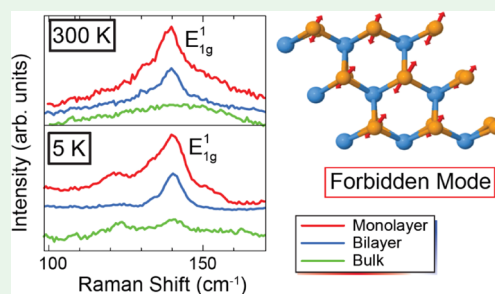
Article Recommendations



Supporting Information

ABSTRACT: Tantalum diselenide (TaSe₂) is a metallic transition metal dichalcogenide whose structure and vibrational behavior strongly depend on temperature and thickness, and this behavior includes the emergence of charge density wave (CDW) states at very low temperatures. In this work, observed Raman modes for mono- and bilayer are described across several spectral regions and compared to those seen in the bulk case. These modes, which include an experimentally observed forbidden Raman mode and low-frequency CDWs, are then matched to corresponding vibrations predicted by density functional theory (DFT). The reported match between experimental and computational results supports the presented vibrational visualizations of these modes. Support is also provided by experimental phonons observed in additional Raman spectra as a function of temperature and thickness. These results highlight the importance of understanding CDWs since they are likely to play a fundamental role in the future realization of solid-state quantum information platforms based on nonequilibrium phenomena.

KEYWORDS: charge density waves, density functional theory, transition metal dichalcogenides, Raman spectroscopy, forbidden mode



INTRODUCTION

Layered two-dimensional (2D) materials are the subject of many research pursuits for their versatile and novel properties.^{1–4} Among those 2D materials, TaSe₂ attracts interest due to its ability to host charge density wave (CDW) states, yielding potential functions in quantum information science.^{5,6} Applications for quantum devices often require fabrication of an atomically thin material to maximize the tunability of the material's properties.⁷ For layered materials, quantum confinement can heavily contribute to any layer-dependent properties. It then follows that a comparison between monolayer (1L), bilayer (2L), and bulk systems should be made to provide a general understanding of what modes emerge and how their behavior differs with thickness.

Generally, layered 2H-TaSe₂ exhibits an incommensurate CDW (IC-CDW) phase between 122 and 90 K as well as a commensurate CDW (C-CDW) phase below 90 K.^{8,9} Also, since the superconducting phase transition of 2H-TaSe₂ occurs at 0.2 K, the corresponding phase does not coexist with the CDW phase, rendering this material an ideal system for studying the layer dependence of these quantum phase transitions. To date, several studies have focused on the evolution of electronic structures and CDW formation,^{10–13} but few explore low-frequency modes.¹⁴ Though various modes in atomically thin 2H-TaSe₂ as well as other similar materials like NbSe₂ are described to some degree by Raman

spectra in other works,^{15–20} many modes elude sufficient visualization, warranting an investigation like the one presented here.^{21–27} A comprehensive examination of these modes with density functional theory (DFT) is crucial to the general understanding of the quantum phenomena seen in these materials systems, such as superconductivity and charge density waves. Furthermore, this quantitative assessment of the observed modes is vital for future efforts to realize solid-state quantum information platforms based on nonequilibrium phenomena.²⁸

In this work, experimental data from Raman spectroscopy and calculated predictions from DFT were used to examine the observed low-frequency CDW modes and the forbidden mode in layered 2H-TaSe₂. Specifically, DFT was used to calculate the appropriate electronic structures of 1L, 2L, and the bulk material until a suitable agreement was found for well-known higher-frequency modes (namely, the E_{2g}¹ and A_{1g} modes). This agreement served as a support for the notion that subsequent modes found in the mid- and low-frequency ranges

Received: December 2, 2020

Accepted: February 9, 2021

could be accurately described by the same DFT model. The various vibrational modes are discussed for both 300 K and temperatures below the CDW phase transitions, with discussions around the temperature-dependent behavior of those modes. Significant differences between the phonons of atomically thin and bulk systems were observed, and these modes are described visually since such descriptions are lacking in the literature.

METHODS AND RESULTS

Calculations were obtained with Quantum ESPRESSO, with the core plane-wave functions provided by the plane-wave self-consistent field (PWscf) component.^{29–31} The Perdew–Zunger (PZ) exchange and correlation functionals were used for the phonon calculations within the applied local density approximations (LDAs).³² Applying LDAs yielded a more accurate description of the optical properties of TaSe₂ than the generalized gradient approximation (GGA), despite the general tendency of LDAs to underestimate the exchange energy and overestimate the correlation energy.³³ Norm-conserving pseudopotentials were used for describing the interactions between the core and valence electrons.^{34,35}

All DFT calculations were done at a thermal temperature of 0 K, but to model the temperature-dependent formation of various Raman modes, the electronic temperature was modulated by tuning the smearing factor σ , a parameter that describes the Fermi–Dirac distribution. The effect of temperature on the phonon properties was also explored.^{36–40} The approach of modeling real temperature effects with electronic temperature variations was validated by computing the lattice expansion as a function of temperature and comparing it with experimental results. Mode frequencies were determined at the gamma point after simulating the predicted electronic and phonon band structure of each material system (1L, 2L, and bulk).

Ground state calculations were performed by relaxing atomic positions and lattice vectors of 1L 2H-TaSe₂ (point group D_{3h}). The optimized lattice constants ($a_{\text{TaSe}_2} = 0.337$ nm and $c_{\text{TaSe}_2} = 1.23$ nm) are within reasonable ranges when compared with other computational studies.^{41,42} The 1L supercell was constructed having nine unit cells ($3 \times 3 \times 1$) and used a sufficiently large vacuum (greater than 20 Å) in the vertical direction to negate any interaction between neighboring supercells. The kinetic energy cutoff of the plane-wave expansion was 520 eV. All geometric structures were fully relaxed until the force on each atom was less than 0.002 eV/Å, and the energy convergence criterion was 10^{-7} eV. For the unit cell and supercell structure relaxation, a $16 \times 16 \times 16$ and $3 \times 3 \times 8$ k -point grid were used, respectively. For the 1L and 2L unit cell and supercell, we used a $16 \times 16 \times 1$ and $9 \times 9 \times 1$ k -point grid, respectively. For phonon calculations, a $4 \times 4 \times 4$ uniform q -grid was used for the unit cell and only performed gamma point phonon calculations for the supercell ($3 \times 3 \times 1$). Further details are included in the Supporting Information. Ultimately, it is this supercell structure that gives the most insight into how the CDW phase equilibrates below the transition temperature. The structure can then be used to calculate phonon and electronic band structures from which Raman transition lines are calculated.

For the experimental data, crystals of 2H-TaSe₂ were grown from Ta metal and Se (99.95 and 99.999% purity, respectively) via iodine vapor transport. The process time ranged from 250 h to 300 h, and the temperature gradient ranged from 600 °C to 620 °C, with the crystals growing within sealed quartz tubes at the cooler end of the furnace. A slight Se excess near 0.2% was included to ensure proper stoichiometry in the final crystals. An illustration of this material growth process and system is provided in Figure 1a. Samples were mechanically exfoliated on Si/SiO₂ substrates (300 nm oxide layer) using adhesive tape to peel the layers off. To prevent issues arising from oxidation and humidity, samples were prepared under an inert nitrogen environment and loaded directly into a gaseous helium-filled cryostat, where it is then cooled to the desired temperature.

During Raman spectrum acquisition, a 515 nm laser excitation was used at sample temperatures between 5 K and 300 K. Both 1L and 2L samples were identified with optical contrast and well-known Raman

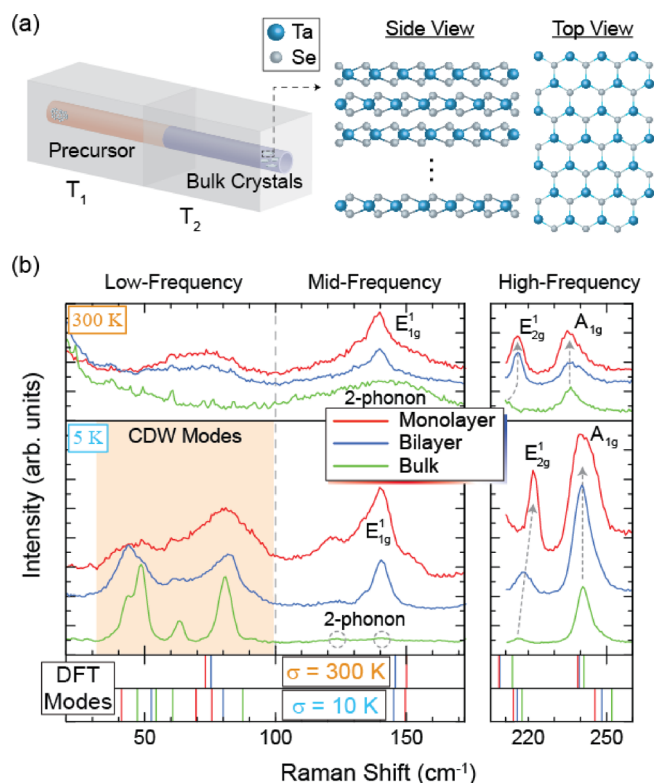


Figure 1. (a) An illustration of the material growth process and the atomic structure of TaSe₂ is shown. (b) Experimental Raman spectra are presented here for the 1L (red curves), 2L (blue curves), and bulk (green curves) TaSe₂ at two temperatures: 300 K (top panel) and 5 K (lower panel). Two vertically shortened panels are displayed at the bottom for DFT modes at the two temperatures with corresponding color schemes. The comparisons of these spectra are subdivided into three intervals: high-, mid-, and low-frequency region. The shaded region in the 5 K measurements highlights the low-frequency CDW modes.

modes (E_{1g} and A_{1g}). Scattered light was collected by using a triple-grating spectrometer to enable low-frequency measurements (with a detection as low as 10 cm⁻¹). The modes in all Raman spectra were characterized by Lorentzian profiles to extract the position and width information, unless otherwise stated.

A comparison of DFT predictions to experimental Raman spectra is shown in Figure 1b, where the predictions were obtained from the calculated structures for the supercell ($3 \times 3 \times 1$) of 2H-TaSe₂, for the 1L, 2L, and bulk cases at endpoint temperatures of 10 and 300 K and compared to Raman spectra obtained at 5 and 300 K. Although bulk 2H-TaSe₂ is predicted to exhibit 12 phonon modes, represented by $\Gamma (D_{6h}) = A_{1g} + 2A_{2u} + B_{1u} + 2B_{2g} + E_{1g} + 2E_{1u} + E_{2u} + 2E_{2g}$, only four are Raman-active: A_{1g}, E_{1g}, and two E_{2g} modes.

The DFT-calculated peak positions, shown in the lowest panel of Figure 1b, align well with the experimental data, providing support for this model in terms of characterizing other lesser-known modes. A discrepancy in the high-frequency data appears between DFT and experimental data. Going from bulk to 1L appears in the data as an increase in frequency, despite the opposite trend being predicted. Similar opposite trends from bulk to few-layer TaSe₂ have also been seen in another DFT work.⁴² Two potential reasons for this discrepancy are the physical presence of a substrate hindering freestanding vibrations (which DFT represents) and the strain imposed from a substrate, which can increase the overall measured frequency of the mode.⁴³

There are several significant changes when transitioning from room temperature (300 K) to below the CDW phase transitions (5 K) that will be detailed in due course. Raman spectra will be evaluated within

each of the following three spectral regions: (a) high-frequency range (above 200 cm^{-1}), (b) mid-frequency range ($100\text{--}175\text{ cm}^{-1}$), and (c) low-frequency range (below 100 cm^{-1}). The exact spectral region bounds were chosen arbitrarily for the sake of orderliness, but the high-frequency range was specifically selected to validate the DFT model used for subsequent descriptions of modes found in the other two spectral regions.

Using the experimental data in Figure 2a as a reference, the evolution of the theoretically predicted high-frequency modes A_{1g} and

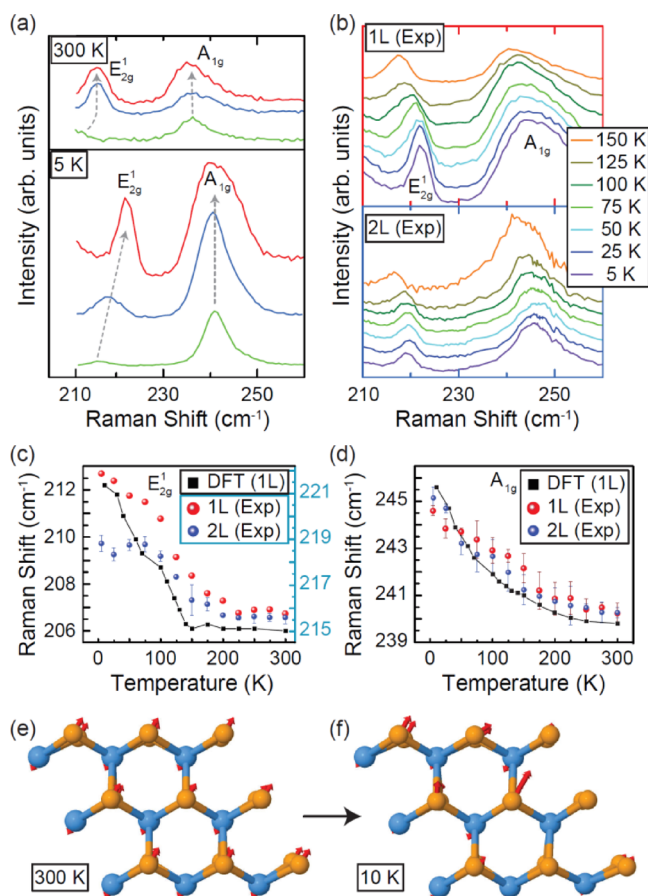


Figure 2. (a) The two experimentally observed high-frequency modes for TaSe₂ are shown for 1L, 2L, and bulk. (b) In the top panel, 1L Raman spectra are shown as a function of temperature. The bottom panel shows the 2L case. (c) The theoretically derived data of the E_{2g}^1 mode is observed to abruptly begin shifting as the temperature decreases (represented by the left vertical axis). Corresponding experimental data are shown with the same data point format and represented by the right vertical axis. (d) The theoretically derived data of the A_{1g} mode is shown as a function of electronic temperature (σ) and compared with experimental data (red and blue circles for 1L and 2L, respectively). The error bars indicate a 1σ standard deviation from the determined peak value using Lorentzian fits and, in some cases, are smaller than the data points. (e) Illustrations of the 1L Ta atoms' (E_{2g}^1) vibration direction are shown at 300 K and (f) 10 K. Note that, despite the appearance of this mode as simply displaying a blueshift with decreasing temperature, its inherent vibrations at the two temperatures are different.

E_{2g}^1 in the 1L case is shown in Figure 2b–d. Both 1L modes display a blueshift with decreasing temperature, similar to their bulk counterparts, though the nature of those modes is inherently different between 1L and bulk, as discussed below. The experimental Raman spectra and DFT results agree within 10 cm^{-1} for the E_{2g}^1 mode and within 2 cm^{-1} for the A_{1g} mode, which exhibited a slightly smaller blueshift than the E_{2g}^1 mode. The differences in the trend for A_{1g} could

be due to the experimental data being taken on a sample mounted on a substrate. This consideration would be consistent with A_{1g} being an out-of-plane mode, thus being strongly influenced by its surrounding environment. Additional polarization data are shown in the Supporting Information.

Another experimental observation was made in the temperature-dependent change of frequency exhibited by the A_{1g} and E_{2g}^1 modes. In the 1L case, the two peaks blueshifted with decreasing temperature by $4.1\text{ cm}^{-1} \pm 1.2\text{ cm}^{-1}$ and $6.2 \pm 0.2\text{ cm}^{-1}$, respectively, where the error indicates a 1σ standard deviation. For the bulk case, those two shifts were $5.0\text{ cm}^{-1} \pm 0.2\text{ cm}^{-1}$ and $6.7\text{ cm}^{-1} \pm 0.2\text{ cm}^{-1}$, respectively. The different behavior between the 1L and bulk temperature-dependent shifts can be explained consistently with results reported in another work.²⁷ To summarize, the A_{1g} mode in 1L (and 2L) experiences a decreased force constant due to a weakening van der Waals force in thin materials, which is why the temperature-dependent shifting of this mode is nearly identical to 1L, 2L, and bulk (to within experimental error). Second, the temperature-dependent shift of the E_{2g}^1 mode is greater in bulk compared to the 1L case, highlighting the decreasing strength of long-range Coulomb interactions as the material became thinner.^{44–46}

The most significant temperature-dependent similarities between the atomically thin material and bulk are the smooth behavior seen in the A_{1g} mode and the abrupt onset behavior observed for the E_{2g}^1 mode. The slope discontinuity seen for the theoretically derived E_{2g}^1 mode in 1L (Figure 2b) as well as that seen theoretically and experimentally in bulk²⁷ is due to the Ta atoms abruptly changing the vibration direction as they approach the CDW phase transition temperature. In Figure 2c and Figure 2d, the 1L E_{2g}^1 mode at 300 K and 10 K, respectively, exhibits a temperature-dependent frequency. For the two temperatures listed, the two corresponding frequencies characterizing the 1L E_{2g}^1 mode are in close spectral proximity, but both frequencies are actually represented by different Ta atom vibration directions. In the 1L case, the emergence of a coherent vibration direction is not as prominent, whereas in the bulk case, all Ta atoms abruptly rotate their vibration direction by 30° as they cross below the critical temperature (122 K). Additional details about the changes in the E_{2g}^1 mode during the CDW phase transition are in the Supporting Information. Overall, the DFT model can be validated by its agreement with the trends seen in the experimental data.

To obtain a clearer understanding of the DFT model used, the total density of states (DOS) was calculated. By comparing the thin and bulk cases in terms of their electronic structure, one can readily explain why some modes in the bulk case should be treated differently than modes in the thin case if such modes are aligned or spectrally neighboring. In Figure 3a, the DOSs for the 1L and bulk systems are shown. From the comparison between the atomically thin and bulk system DOS, one may conclude that there are significant changes at the Fermi level and that significant contributions originate from the d-orbital of the Ta atoms (see Figure 3b and the Supporting Information for other partial DOS calculations for p- and d-orbitals). The most obvious change, other than temperature-dependent changes in the DOS with 1L, is the DOS minimum that forms more clearly in the 1L case. Such differences in the electronic structure are attributable to the differences in the structural phase that occur in the thin case versus the bulk case.⁴⁷ For instance, the bulk case is known to have a striped formation at cold temperatures whereas the thin cases are thought to adopt a more triangular formation.⁴⁷ The Ta atoms' contribution to the DOS strongly depends on the position of the atoms, and the contributions are in the far lower energies of the valance band (see the Supporting Information).⁴⁷ As for the bulk case, Ta atoms in striped formations do not contribute to the DOS.²⁷

The same DFT model is used to gain a better understanding of the mid-frequency range of the Raman spectra, where experimental data show the emergence of a forbidden mode (E_{1g}^1) present in the 1L and 2L Raman spectra but not in the bulk spectrum (Figure 4a). At room temperature, there appears to be an overlapping of the E_{1g}^1 and two-phonon modes (dominant in the bulk but not in the 1L spectrum), whereas at 5 K, the overlap becomes less apparent, with the E_{1g}^1 mode becoming more accentuated and the two-phonon mode in bulk

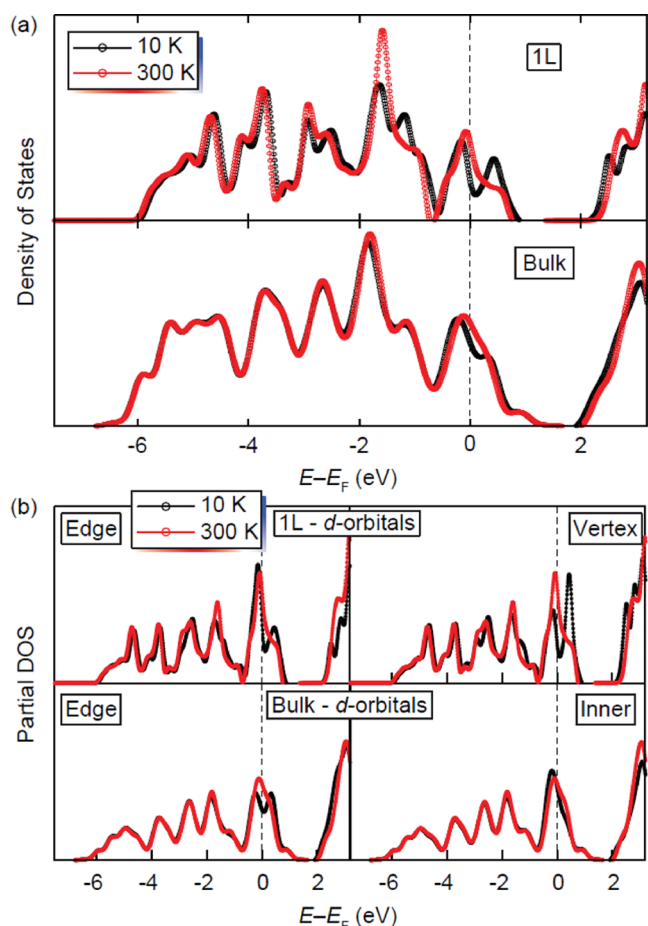


Figure 3. (a) The total densities of states (DOSs) of the d-orbitals of Ta atoms for the 1L and bulk systems are shown in the top and bottom panel, respectively. Furthermore, the DOSs at 300 K and 10 K are calculated and plotted in red and black curves, respectively. (b) The partial densities of states (PDOSs) of the d-orbitals of Ta atoms are shown for the 1L and bulk systems in the top and bottom panels, respectively. Within each thickness, the left panel shows the PDOS for an edge atom whereas the right panel shows either the vertex (1L) or inner (bulk) atom. From the comparison between the 1L and bulk DOS and PDOS, one may see significant changes at the Fermi level, with significant contributions coming from the d-orbital of the Ta atoms.

becoming more distinct.^{48–51} The position and intensity of the forbidden E_{1g}^1 mode in the 1L and 2L cases were found to be temperature-independent (see the Supporting Information). The DFT-calculated position of the E_{1g}^1 mode is 149.4 cm^{-1} (at 10 K), and this agrees well with the previously reported experimental 1L work.⁴⁴ The evolution of the temperature-dependent two-phonon mode for bulk 2H-TaSe₂ systems has been discussed in a recent publication.²⁷ One explanation for the observation of a forbidden E_{1g}^1 mode in the 2D limit is the introduction of a broken symmetry in the 1L case (lack of a periodic third dimension).⁴⁸ For the case of 2L, the same argument holds, though to a slightly lesser extent. The broken symmetry still exists with a second layer, though the intensity is not as high. As shown in Figure 4b,c, the visualization of the forbidden mode does not appear to change with the addition of a second layer, despite the slight redshift in both DFT and experimental data.

Last, results for the low-frequency region are examined in Figure 5a. The experimental 1L and 2L spectra are superposed with three DFT-calculated modes most likely to describe the observed behavior. These modes result from phonon zone folding due to the superlattice structure present in the CDW phase, as is expected from changing lattice periodicities. The lowest-frequency mode is predicted at 41.7

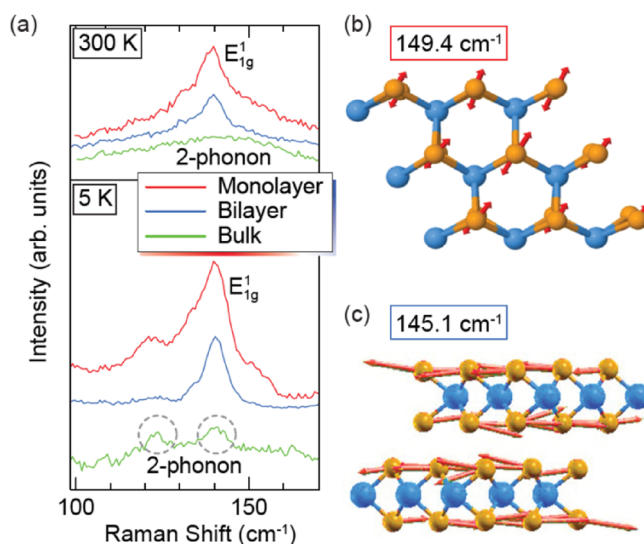


Figure 4. (a) Experimentally observed Raman spectra of 1L, 2L, and bulk for the mid-frequency range. (b) The forbidden mode for 1L is visualized here and compared with panel (c), which is the side view visualization of the 2L forbidden mode. Both visualizations appear very similar, despite the slight redshift in both DFT and experimental data with an added layer.

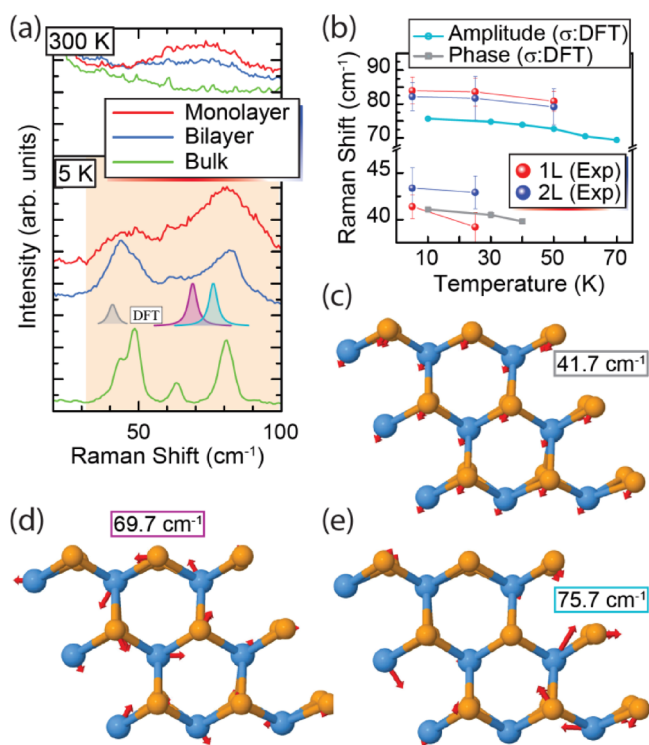


Figure 5. (a) The experimental Raman spectra from the low-frequency region are shown vertically translated. (b) Two modes in the 1L case are calculated as a function of electronic temperature (σ) and determined to be a phase and amplitude mode. The DFT predictions are compared with 1L and 2L extracted mode positions, with errors bars indicating a 1σ standard deviation from the Lorentzian fits. (c–e) Corresponding illustrations of the 1L low-frequency modes calculated with DFT are shown in order of increasing frequency, determined at a set electronic temperature of 10 K.

cm^{-1} and attributed to a phase mode, which exhibits a translational behavior with all atomic layers vibrating in the same direction.²⁷ The

mode emerges at 40 K in the C-CDW phase and blueshifts as the temperature decreases, as shown in Figure 5b. Experimental Raman data were taken in steps of 25 K. Data at 50 K for both the 1L and 2L systems does not show this phase mode, indicating that the emergence temperature is between 25 K and 50 K. An illustration of the phase mode is shown in Figure 5c. The second mode, as shown in Figure 5d, is a circular mode at 69.7 cm^{-1} , and it is independent of temperature and atomic displacement. The third and final mode predicted in 1L TaSe₂, as shown in Figure 5e, emerges near 70 K and blueshifts with decreasing temperature and can be described as an amplitude mode, taking on a more distorted form of circular vibration in the opposite direction to the mode at 69.7 cm^{-1} .²⁷ The predicted temperature-dependent behavior of this third mode in 1L is shown in light blue, with the experimental data for both 1L and 2L showing a similar trend. The Raman spectra taken at 75 K did not appear to include this mode, falling in line with the DFT prediction.

In the bulk case, four modes emerge corresponding to CDWs—two phase and two amplitude modes with larger intensities than the Raman A_{1g} and E_{2g} modes.²⁷ Though the 1L and 2L modes in this region have intensities similar to their bulk counterparts, it is important to note that the bulk modes are completely different lattice modes than those in the 1L or 2L spectra. These differences arise from the changes in the phonon and electronic band structure, which also yield differences in the DOS between bulk and thin cases (see Figure 3). For all four modes in the bulk case, the Se atoms are vibrating in opposite directions to each other and the Ta atoms do not vibrate at all. However, in the atomically thin case, all atoms are vibrating in some ordered fashion.^{52,53} It should be noted that the differences in CDW appearance and why these modes have different vibrational properties stem primarily from the atomic structure that is adopted by the material when entering the CDW phase. As was mentioned earlier, the bulk case is known to adopt a striped lattice formation underneath the CDW phase transition temperature.²⁷ The thin cases are thought to adopt a more triangular lattice for their transition, but this topic on explicit layer dependence of CDW formation is a topic of an ongoing work.⁴⁷

CONCLUSIONS

In this work, observed low-frequency CDWs and the forbidden mode in layered 2H-TaSe₂ were examined via Raman spectroscopy and DFT. Experimental data from the more well-known high-frequency modes (E_{2g} and A_{1g} modes) in 1L, 2L, and bulk TaSe₂ were compared with DFT predictions to validate a suitable model for exploring modes not fully elucidated in the literature. Consequently, modes found in the mid- and low-frequency ranges were accurately described by the same DFT model, with the various vibrational modes discussed for temperatures between 300 K and 5 K. The significant differences observed between the modes of atomically thin and bulk systems were subsequently rendered visually. Overall, the methods underlying this work can be extended to describe and visualize modes in other 2D materials. In all cases, such investigations are necessary for future technologies that rely on CDWs. Most relevantly, control of CDWs or superconducting modes within these materials can open up new tunable degrees of freedom, enabling the development of solid-state quantum information systems based on nonequilibrium phenomena.

ASSOCIATED CONTENT

Supporting Information

The Supporting Information is available free of charge at <https://pubs.acs.org/doi/10.1021/acsnm.0c03222>.

Crystal structure of bulk and monolayer 2H-TaSe₂, structural parameters, temperature-dependent evolution,

PDOS for orbitals, and polarization-dependent Raman spectra (PDF)

AUTHOR INFORMATION

Corresponding Author

Francesca Tavazza — National Institute of Standards and Technology (NIST), Gaithersburg, Maryland 20899, United States; Email: francesca.tavazza@nist.gov

Authors

Sugata Chowdhury — National Institute of Standards and Technology (NIST), Gaithersburg, Maryland 20899, United States; Department of Physics and Astronomy, Howard University, Washington, D.C. 20059, United States

Heather M. Hill — National Institute of Standards and Technology (NIST), Gaithersburg, Maryland 20899, United States

Albert F. Rigosi — National Institute of Standards and Technology (NIST), Gaithersburg, Maryland 20899, United States; orcid.org/0000-0002-8189-3829

Andrew Briggs — National Institute of Standards and Technology (NIST), Gaithersburg, Maryland 20899, United States

Helmuth Berger — École Polytechnique Fédérale de Lausanne (EPFL), Institut de Physique des Nanostructures, CH-1015 Lausanne, Switzerland

David B. Newell — National Institute of Standards and Technology (NIST), Gaithersburg, Maryland 20899, United States

Angela R. Hight Walker — National Institute of Standards and Technology (NIST), Gaithersburg, Maryland 20899, United States; orcid.org/0000-0003-1385-0672

Complete contact information is available at:

<https://pubs.acs.org/10.1021/acsnm.0c03222>

Author Contributions

S.C. performed all theoretical calculations. H.M.H. and A.F.R. performed the experiments and prepared the samples. A.B. and H.B. provided the material. D.B.N., A.R.H.W., and F.T. assisted with the analyses, support, and general project oversight. The manuscript was written through contributions of all authors.

Funding

Support was provided by the National Science Foundation through grant DMR-180119. Work presented herein was performed, for a subset of the authors, as part of their official duties for the U.S. government. Funding is hence appropriated by the U.S. Congress directly.

Notes

The authors declare no competing financial interest.

ACKNOWLEDGMENTS

The authors would like to thank S. Payagala and A. Bicchieri for their assistance in the NIST internal review process.

REFERENCES

- (1) Chhowalla, M.; Jena, D.; Zhang, H. Two-dimensional semiconductors for transistors. *Nat. Rev. Mater.* **2016**, *1*, 16052.
- (2) Mannix, A. J.; Kiraly, B.; Hersam, M. C.; Guisinger, N. P. Synthesis and chemistry of elemental 2D materials. *Nat. Rev. Chem.* **2017**, *1*, 0014.

- (3) Novoselov, K. S.; Geim, A. K.; Morozov, S. V.; Jiang, D.; Katsnelson, M. I.; Grigorieva, I. V.; Dubonos, S. V.; Firsov, A. A. Two-dimensional gas of massless Dirac fermions in graphene. *Nature* **2005**, *438*, 197.
- (4) Novoselov, K. S.; Geim, A. K.; Morozov, S. V.; Jiang, D.; Zhang, Y.; Dubonos, S. V.; Grigorieva, I. V.; Firsov, A. A. Electric Field Effect in Atomically Thin Carbon Films. *Science* **2004**, *306*, 666–669.
- (5) Fröhlich, H. On the theory of superconductivity: The one-dimensional case. *Proc. R. Soc. Lond. A* **1954**, *223*, 296–305.
- (6) Thorne, R. E. Charge-density-wave conductors. *Phys. Today* **1996**, *49*, 42–47.
- (7) Kang, S.; Lee, D.; Kim, J.; Capasso, A.; Kang, H. S.; Park, J.-W.; Lee, C.-H.; Lee, G.-H. 2D semiconducting materials for electronic and optoelectronic applications: potential and challenge. *2D Mater.* **2020**, *7*, No. 022003.
- (8) Moncton, D. E.; Axe, J. D.; DiSalvo, F. J. Study of Superlattice Formation in 2H-NbSe₂ and 2H-TaSe₂ by Neutron Scattering. *Phys. Rev. Lett.* **1975**, *34*, 734.
- (9) Sugai, S.; Murase, K. Generalized electronic susceptibility and charge-density waves in 2H-TaSe₂ by Raman scattering. *Phys. Rev. B* **1982**, *25*, 2418.
- (10) Bawden, L.; Cooil, S. P.; Mazzola, F.; Riley, J. M.; Collins-McIntyre, L. J.; Sunko, V.; Hunvik, K. W. B.; Leandersson, M.; Polley, C. M.; Balasubramanian, T.; Kim, T. K.; Hoesch, M.; Wells, J. W.; Balakrishnan, G.; Bahramy, M. S.; King, P. D. C. Spin–valley locking in the normal state of a transition-metal dichalcogenide superconductor. *Nat. Commun.* **2016**, *7*, 11711.
- (11) Ugeda, M. M.; Bradley, A. J.; Zhang, Y.; Onishi, S.; Chen, Y.; Ruan, W.; Ojeda-Aristizabal, C.; Ryu, H.; Edmonds, M. T.; Tsai, H.-Z.; Riss, A.; Mo, S.-K.; Lee, D.; Zettl, A.; Hussain, Z.; Shen, Z.-X.; Crommie, M. F. Characterization of collective ground states in single-layer NbSe₂. *Nat. Phys.* **2016**, *12*, 92.
- (12) Xi, X.; Wang, Z.; Zhao, W.; Park, J.-H.; Law, K. T.; Berger, H.; Forró, L.; Shan, J.; Mak, K. F. Ising pairing in superconducting NbSe₂ atomic layers. *Nat. Phys.* **2016**, *12*, 139.
- (13) Soumyanarayanan, A.; Yee, M. M.; He, Y.; Van Wezel, J.; Rahn, D. J.; Rossnagel, K.; Hudson, E. W.; Norman, M. R.; Hoffman, J. E. Quantum phase transition from triangular to stripe charge order in NbSe₂. *Proc. Natl. Acad. Sci. U. S. A.* **2013**, *110*, 1623–1627.
- (14) Wang, Q.; Zhang, Q.; Zhang, Q.-W.; Li, X.; Zhao, C.-X.; Xu, T.-Y.; Qu, D.-H.; Tian, H. Color-tunable single-fluorophore supramolecular system with assembly-encoded emission. *Nat. Commun.* **2020**, *11*, 158.
- (15) Xi, X.; Zhao, L.; Wang, Z.; Berger, H.; Forró, L.; Shan, J.; Mak, K. F. Strongly enhanced charge-density-wave order in monolayer NbSe₂. *Nat. Nanotechnol.* **2015**, *10*, 765.
- (16) Yu, Y.; Yang, F.; Lu, X. F.; Yan, Y. J.; Cho, Y.-H.; Ma, L.; Niu, X.; Kim, S.; Son, Y.-W.; Feng, D.; Li, S.; Cheong, S.-W.; Chen, X. H.; Zhang, Y. Gate-tunable phase transitions in thin flakes of 1T-TaS₂. *Nat. Nanotechnol.* **2015**, *10*, 270–276.
- (17) Yoshida, M.; Suzuki, R.; Zhang, Y.; Nakano, M.; Iwasa, Y. Memristive phase switching in two-dimensional 1T-TaS₂ crystals. *Sci. Adv.* **2015**, *1*, No. e1500606.
- (18) Yang, J.; Wang, W.; Liu, Y.; Du, H.; Ning, W.; Zheng, G.; Jin, C.; Han, Y.; Wang, N.; Yang, Z.; Tian, M.; Zhang, Y. Thickness dependence of the charge-density-wave transition temperature in VSe₂. *Appl. Phys. Lett.* **2014**, *105*, No. 063109.
- (19) Hu, S. G.; Liu, Y.; Liu, Z.; Chen, T. P.; Wang, J. J.; Yu, Q.; Deng, L. J.; Yin, Y.; Hosaka, S. Associative memory realized by a reconfigurable memristive Hopfield neural network. *Nat. Commun.* **2015**, *6*, 7522.
- (20) Feng, J.; Biswas, D.; Rajan, A.; Watson, M. D.; Mazzola, F.; Clark, O. J.; Underwood, K.; Marković, I.; McLaren, M.; Hunter, A.; Burn, D. M.; Duffy, L. B.; Barua, S.; Balakrishnan, G.; Bertran, F.; le Fèvre, P.; Kim, T. K.; van der Laan, G.; Hesjedal, T.; Wahl, P.; King, P. D. C. Electronic Structure and Enhanced Charge-Density Wave Order of Monolayer VSe₂. *Nano Lett.* **2018**, *18*, 4493–4499.
- (21) Bhatt, R. N.; McMillan, W. L. Theory of phonon dynamics near a charge-density-wave instability. *Phys. Rev. B* **1975**, *12*, 2042.
- (22) Borisenko, S. V.; Kordyuk, A. A.; Yaresko, A. N.; Zabolotnyy, V. B.; Inosov, D. S.; Schuster, R.; Büchner, B.; Weber, R.; Follath, R.; Patthey, L.; Berger, H. Pseudogap and charge density waves in two dimensions. *Phys. Rev. Lett.* **2008**, *100*, 196402.
- (23) Holy, J. A.; Klein, M. V.; McMillan, W. L.; Meyer, S. F. Raman-Active Lattice Vibrations of the Commensurate Superlattice in 2H-TaSe₂. *Phys. Rev. Lett.* **1976**, *37*, 1145.
- (24) Rossnagel, K.; Rotenberg, E.; Koh, H.; Smith, N. V.; Kipp, L. Fermi surface, charge-density-wave gap, and kinks in 2H-TaSe₂. *Phys. Rev. B* **2005**, *72*, 121103.
- (25) Rossnagel, K.; Smith, N. V. Spin-orbit splitting, Fermi surface topology, and charge-density-wave gapping in 2H-TaSe₂. *Phys. Rev. B* **2007**, *76*, No. 073102.
- (26) Tsang, J. C.; Smith, J. E., Jr.; Shafer, M. W. Effect of charge density wave fluctuations on the frequencies of optic phonons in 2H-TaSe₂ and-NbSe₂. *Solid State Commun.* **1978**, *27*, 145–149.
- (27) Hill, H. M.; Chowdhury, S.; Simpson, J. R.; Rigosi, A. F.; Newell, D. B.; Berger, H.; Tavazza, F.; Walker, A. R. H. Phonon origin and lattice evolution in charge density wave states. *Phys. Rev. B* **2019**, *99*, 174110.
- (28) Head-Marsden, K.; Flick, J.; Ciccarino, C. J.; Narang, P. Quantum Information and Algorithms for Correlated Quantum Matter. *Chem. Rev.* **2020**, DOI: 10.1021/acs.chemrev.0c00620.
- (29) Hohenberg, P.; Kohn, W. Inhomogeneous electron gas. *Phys. Rev.* **1964**, *136*, B864.
- (30) Kohn, W.; Sham, L. J. Self-consistent equations including exchange and correlation effects. *Phys. Rev.* **1965**, *140*, A1133.
- (31) Giannozzi, P.; Baroni, S.; Bonini, N.; Calandra, M.; Car, R.; Cavazzoni, C.; Ceresoli, D.; Chiarotti, G. L.; Cococcioni, M.; Dabo, I.; Dal Corso, A.; de Gironcoli, S.; Fabris, S.; Fratesi, G.; Gebauer, R.; Gerstmann, U.; Gougoussis, C.; Kokalj, A.; Lazzeri, M.; Martin-Samos, L.; Marzari, N.; Mauri, F.; Mazzarello, R.; Paolini, S.; Pasquarello, A.; Paulatto, L.; Sbraccia, C.; Scandolo, S.; Sclauzero, G.; Seitsonen, A. P.; Smogunov, A.; Umari, P.; Wentzcovitch, R. M. QUANTUM ESPRESSO: a modular and open-source software project for quantum simulations of materials. *J. Phys. Condens. Mater.* **2009**, *21*, 395502.
- (32) Perdew, J. P.; Zunger, A. Self-interaction correction to density-functional approximations for many-electron systems. *Phys. Rev. B* **1981**, *23*, 5048.
- (33) Perdew, J. P.; Chevary, J. A.; Vosko, S. H.; Jackson, K. A.; Pederson, M. R.; Singh, D. J.; Fiolhais, C. Atoms, molecules, solids, and surfaces: Applications of the generalized gradient approximation for exchange and correlation. *Phys. Rev. B* **1992**, *46*, 6671.
- (34) Fuchs, M.; Scheffler, M. Ab initio pseudopotentials for electronic structure calculations of poly-atomic systems using density-functional theory. *Comput. Phys. Commun.* **1999**, *119*, 67–98.
- (35) Troullier, N.; Martins, J. L. Efficient pseudopotentials for plane-wave calculations. *Phys. Rev. B* **1991**, *43*, 1993.
- (36) Calandra, M.; Mazin, I. I.; Mauri, F. Effect of dimensionality on the charge-density wave in few-layer 2H-NbSe₂. *Phys. Rev. B* **2009**, *80*, 241108.
- (37) Duong, D. L.; Burghard, M.; Schön, J. C. Ab initio computation of the transition temperature of the charge density wave transition in TiSe₂. *Phys. Rev. B* **2015**, *92*, 245131.
- (38) Gruner, G. *Density waves in solids*; CRC Press: 2018
- (39) Kohn, W. Image of the Fermi Surface in the Vibration Spectrum of a Metal. *Phys. Rev. Lett.* **1959**, *2*, 393.
- (40) Motizuki, K.; Suzuki, N.; Yoshida, Y.; Takaoka, Y. Role of electron-lattice interaction in lattice dynamics and lattice instability of 1T-TiSe₂. *Solid State Commun.* **1981**, *40*, 995–998.
- (41) Weber, F.; Rosenkranz, S.; Castellán, J.-P.; Osborn, R.; Hott, R.; Heid, R.; Bohnen, K.-P.; Egami, T.; Said, A. H.; Reznik, D. Extended Phonon Collapse and the Origin of the Charge-Density Wave in 2H-NbSe₂. *Phys. Rev. Lett.* **2011**, *107*, 107403.
- (42) Yan, J.-A.; Cruz, M. A. D.; Cook, B.; Varga, K. Structural, electronic and vibrational properties of few-layer 2H- and 1T-TaSe₂. *Sci. Rep.* **2015**, *5*, 16646.

- (43) Wu, X.; Cai, Y.; Bian, J.; Su, G.; Luo, C.; Yang, Y.; Zhang, G. Strain engineering and lattice vibration manipulation of atomically thin TaS₂ films. *RSC Adv.* **2020**, *10*, 16718.
- (44) Hajiyeve, P.; Cong, C.; Qiu, C.; Yu, T. Contrast and Raman spectroscopy study of single-and few-layered charge density wave material: 2H-TaSe₂. *Sci. Rep.* **2013**, *3*, 2593.
- (45) Liang, L.; Meunier, V. First-principles Raman spectra of MoS₂, WS₂ and their heterostructures. *Nanoscale* **2014**, *6*, 5394–5401.
- (46) Saito, R.; Tatsumi, Y.; Huang, S.; Ling, X.; Dresselhaus, M. S. Raman spectroscopy of transition metal dichalcogenides. *J. Phys. Condens. Matter* **2016**, *28*, 353002.
- (47) Chowdhury, S.; Rigosi, A. F.; Hill, H. M.; Briggs, A.; Newell, D. B.; Berger, H.; Walker, A. R.; Tavazza, F. Effect of van der Waals Interactions on Quantum Phase Transitions and Resulting Phonon Properties of 2H-TaSe₂. arXiv preprint arXiv:200511350 2020 May 22 2020
- (48) Froehlicher, G.; Lorchat, E.; Fernique, F.; Joshi, C.; Molina-Sánchez, A.; Wirtz, L.; Berciaud, S. Unified Description of the Optical Phonon Modes in N-Layer MoTe₂. *Nano Lett.* **2015**, *15*, 6481–6489.
- (49) Guo, Y.; Zhang, W.; Wu, H.; Han, J.; Zhang, Y.; Lin, S.; Liu, C.; Xu, K.; Qiao, J.; Ji, W.; Chen, Q.; Gao, S.; Zhang, W.; Zhang, X.; Chai, Y. Discovering the forbidden Raman modes at the edges of layered materials. *Sci. Adv.* **2018**, *4*, No. eaau6252.
- (50) Nam, D.; Lee, J.-U.; Cheong, H. Excitation energy dependent Raman spectrum of MoSe₂. *Sci. Rep.* **2015**, *5*, 17113.
- (51) Scheuschner, N.; Gillen, R.; Staiger, M.; Maultzsch, J. Interlayer resonant Raman modes in few-layer MoS₂. *Phys. Rev. B* **2015**, *91*, 235409.
- (52) Snow, C. S.; Karpus, J. F.; Cooper, S. L.; Kidd, T. E.; Chiang, T.-C. Quantum Melting of the Charge-Density-Wave State in 1T-TiSe₂. *Phys. Rev. Lett.* **2003**, *91*, 136402.
- (53) Singh, B.; Hsu, C.-H.; Tsai, W.-F.; Pereira, V. M.; Lin, H. Stable charge density wave phase in a 1T-TiSe₂ monolayer. *Phys. Rev. B* **2017**, *95*, 245136.